Microscopic simulations of fracture dissolution

P. Szymczak

Institute of Theoretical Physics, Warsaw University, Warsaw, Poland

A. J. C. Ladd

Chemical Engineering Department, University of Florida, Gainesville, Florida, USA

[1] Microscopic simulations of fracture dissolution are reported, taking account of the explicit topography of the pore space, the transport of reactants and products, and the chemical kinetics at the solid surfaces. A three-dimensional numerical model has been constructed, in which the fluid velocity field is calculated with an implicit lattice-Boltzmann method, and the transport of dissolved species is modeled by an innovative random walk algorithm that incorporates the chemical kinetics at the solid surfaces. The model contains no free parameters or semi-empirical mass-transfer coefficients. The simulated morphological changes in a complex fracture are compared with recent laboratory experiments [*Detwiler et al.*, 2003] with the same initial topography. *INDEX TERMS:* 1832 Hydrology: Groundwater transport; 1869 Hydrology: Stochastic processes; 3230 Mathematical Geophysics: Numerical solutions; 5104 Physical Properties of Rocks: Fracture and flow; 5114 Physical Properties of Rocks: Permeability and porosity. **Citation:** Szymczak, P., and A. J. C. Ladd (2004), Microscopic simulations of fracture dissolution, *Geophys. Res. Lett.*, *31*, L23606, doi:10.1029/2004GL021297.

1. Introduction

[2] The dissolution of a fractured rock by a reactive fluid depends on a subtle interplay between chemical reactions at mineral surfaces and fluid motion in the pores. The complex geometry of a typical fracture makes a first-principles calculation very demanding, and models of fracture dissolution are rarely constructed on a microscopic (pore-scale) level (but see *Békri et al.* [1997] and *Verberg and Ladd* [2002]). Instead, various approximations are resorted to in order to make the analysis more tractable. For example, the Reynolds (or lubrication) approximation is often used [*Groves and Howard*, 1994; *Adler and Thovert*, 2000; *Cheung and Rajaram*, 2002], although it has been shown [*Brown et al.*, 1995; *Oron and Berkowitz*, 1998; *Nicholl et al.*, 1999] that it may significantly overestimate the flow rate, especially for fractures of high roughness and small apertures. Furthermore, the transport of dissolved material into the bulk of the fluid is usually accounted for in a simplified way, with the effects of convection in the fracture assumed to be adequately expressed by a Sherwood number for transport in ducts [*Groves and Howard*, 1994; *Dreybrodt*, 1996; *Cheung and Rajaram*, 2002]. However fracture erosion is a complex process involving several nonlinear feedback mechanisms, which makes it hard to estimate or control the effects of approximations. Recent advances in numerical algorithms for flow and transport [*Verberg and Ladd*, 1999, 2000; *Szymczak and Ladd*, 2004] now make it feasible to simulate systems of relevance to laboratory experiments without resorting to semi-empirical approximations. Instead the fundamental equations for fluid flow, transport of reactants and products, and chemical kinetics are solved directly. The simulations incorporate the explicit topography of the pore space, and the transport coefficients – viscosity, diffusivity, and reaction rate – are determined independently, so there are no fitting parameters. In this work we will describe an application to the erosion of a synthetic fracture. The simulations account for the key features of the experimental erosion patterns as well as the statistical distribution of the depth of erosion. Our results suggest that fully microscopic simulations can be a useful tool in the development of Darcy scale models of dissolution.

2. KDP Fracture

[3] We have studied the dissolution of the artificial fracture system investigated experimentally by *Detwiler et al.* [2003]. The system was created by mating a 99 × 152 mm plate of textured glass (spatial correlation length of ∼0.8 mm) with a flat, transparent plate of potassium-dihydrogen-phosphate (KDP). Since only the KDP surface dissolves, it is possible to repeat the experiment with identical initial conditions by mating the same glass surface with another flat KDP plate. The relative position of the two surfaces was fixed during the experiment, eliminating the effects of confining pressure, which are hard to control experimentally [*Durham et al.*, 2001] and even harder to model numerically in an unambiguous way [*Verberg and Ladd*, 2002].

[4] Constant head reservoirs were connected to each end of the fracture to generate hydraulic gradients of 4% and 16%, corresponding to initial values of the Peclet number, $Pe = Uh_0/D$, of 54 and 216 respectively. Here U is a characteristic fluid velocity, h_0 is the initial mean aperture and D is the solute diffusion coefficient (for KDP in water $D = 6.8 \cdot 10^{-10}$ m^2 s^{-1}). The mean velocity $U = Q/wh_0$, is determined from the flow rate, Q, and the mean cross section of the fracture, wh_0, where w is the fracture width. The fracture was dissolved by an inflowing solution of KDP at 5% undersaturation. High spatial resolution data (1192 × 1837, 0.083 × 0.083 mm pixels) was obtained by *Detwiler et al.* [2003] for the change in fracture aperture as a function of spatial position. The experiments were continued until the mean aperture of $h_0 = 0.126$ mm increased approximately twofold; i.e., $\Delta h \sim h_0$, with

Δh being the difference between the final and initial aperture.

3. Numerical Simulation Method

[5] The numerical simulations consist of a sequence of three separate calculations. First the fluid flow field in the pore space is calculated, using the exact topography of the solid surface. Given the flow field and the chemical kinetics at the solid surfaces, we first determine the solute concentration field and then the local rate of dissolution over the whole fracture surface. Finally the fracture surfaces are eroded in proportion to the local dissolution rate and the whole process is repeated. The key assumption here is that the relaxation times of the velocity and concentration fields are much shorter than the characteristic relaxation time for dissolution. Within this quasi-static approximation, the velocity and concentration fields in the fracture reach a steady state for each configuration.

3.1. Flow Field Calculation

[6] The Reynolds number $Re = \rho U h_0/\eta$ characterizing the flow in laboratory-scale fractures [*Durham et al.*, 2001; *Dijk et al.*, 2002; *Detwiler et al.*, 2003] is typically less than 1. Thus, inertia can be neglected and fluid motion is then governed by the Stokes equations

$$\nabla \cdot \mathbf{u} = 0; \quad \eta \nabla^2 \mathbf{u} = \nabla p, \qquad (1)$$

where $\mathbf{u}$ is the fluid velocity, η is the viscosity and p is the pressure. The velocity field in the fracture has been calculated using the lattice-Boltzmann method with ''continuous bounce-back'' rules applied at the solid-fluid boundaries [*Verberg and Ladd*, 2000]. These rules allow the solid surface to be resolved on length scales less than a grid spacing, so that the fracture surfaces erode smoothly. It has been shown [*Verberg and Ladd*, 2002] that the flow fields in rough fractures can be calculated with one-half to one-quarter the linear resolution of the traditional lattice Boltzmann method, leading to an order of magnitude reduction in memory and computation time. A further order of magnitude saving in computation time can be obtained by solving equation (1) directly by conjugate gradients [*Verberg and Ladd*, 1999] rather than by time stepping. These improvements allow us to calculate velocity fields in fractures with a characteristic size of several centimeters. For example, the calculation of a single flow field in the KDP fracture described above takes 1 hour at the beginning and about 8 hours at the final stages of the dissolution process. The corresponding times for the traditional lattice Boltzmann method would be measured in weeks rather than hours.

[7] Computational limitations imposed by our single-processor flow simulator mean that the spatial resolution of the pore space is limited, and the mean aperture of the initial fracture corresponds to about 1.5 grid spacings. We therefore carried out test calculations on a subsection of the fracture, comparing dissolution patterns for grid spacings of 0.083 mm and 0.0415 mm. The overall features of the dissolution patterns were found to be similar although there were differences in the small-scale details.

[8] The permeability of the initial fracture was calculated at 0.083 mm resolution and then non-dimensionalized by the mean aperture, h_0. The dimensionless permeability for the simulated fracture was found to be $K/h_0^2 = 0.1$, while an estimate based on the experimental data was lower, $K/h_0^2 = 0.05$ [*Detwiler et al.*, 2003]. The experimental measurement is known to be low, since the pressure drop was measured across the whole apparatus, not just the fracture. In view of this and the coarse resolution of the simulated flow field, the agreement is reasonable.

3.2. Solute Transport Modeling

[9] Solute transport in the fracture is modeled by a random walk algorithm that takes explicit account of the chemical reactions at the pore surfaces. We thereby obtained a stochastic solution to the convection-diffusion equation,

$$\partial_t c + \mathbf{u} \cdot \nabla c = D\nabla^2 c, \qquad (2)$$

with the flow field, $\mathbf{u}$, derived from the lattice-Boltzmann simulation and boundary conditions determined by the local dissolution flux. The drawback of the classical random walk method [*Békri et al.*, 1995] is that a very large number of particles must be tracked simultaneously, so that the concentration near the pore surface can be determined accurately enough to obtain a statistically meaningful dissolution flux. However, there is a considerable simplification for linear dissolution kinetics, where the erosion flux through the interface is given by

$$J = r(c_s - c_0); \qquad (3)$$

here c_0 denotes the solute concentration at the interface, c_s is the saturation concentration, and r the rate constant. In this case it is possible to derive a single-particle stochastic propagator which satisfies the boundary condition in equation (3) [*Szymczak and Ladd*, 2004]. Using this propagator, the dissolution flux in the fracture can be calculated by tracking a single particle at a time. Each particle undergoes many encounters with the fracture surface, losing mass on each encounter according to the rate constant. This scheme is computationally more efficient by several orders of magnitude than one which requires local concentration measurements, and can be used to calculate the concentration profiles in very large fractures. The changes in fracture morphology are then realized by removing material from the fracture walls in proportion to the local dissolution flux calculated in the random walk step. The time evolution of the velocity field and local aperture are determined by iteration, removing small amounts of material (equivalent to a layer of about 1% of the mean aperture) at each step and then recalculating the flow field and concentration field for each new geometry.

3.3. Dissolution Kinetics

[10] According to [*Koziejowska and Sangwal*, 1988], the KDP dissolution kinetics can be adequately described by a birth-and-spread model [*Ohara and Reid*, 1973]. In the undersaturation range 0–6% the dissolution flux is then given by

$$J = A(1 - c_0/c_s)^{5/6} \exp(-B/(1 - c_0/c_s)), \qquad (4)$$

where the parameters A and B depend in particular on the temperature and crystal geometry. To apply our random
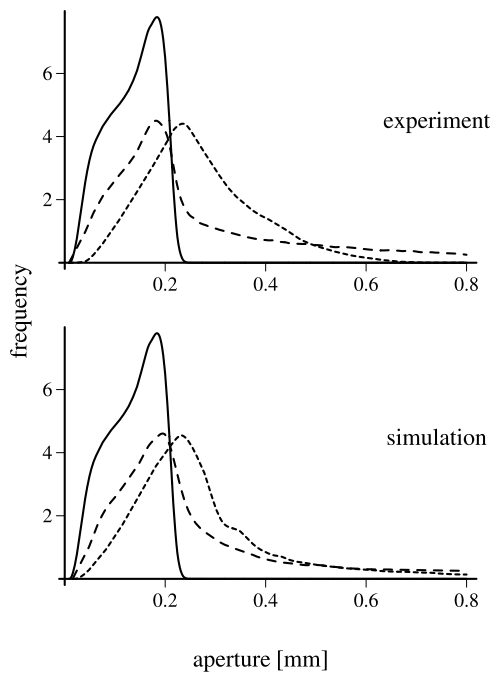
Figure 1. Histograms of aperture distributions at different Peclet numbers. The solid line is the initial aperture distribution, while the dashed and dotted lines are final aperture distributions at $Pe = 54$ and $Pe = 216$ respectively.

walk method, the dissolution kinetics are approximated by a linear function of the form in equation (3). From the experimental data [*Koziejowska and Sangwal*, 1988] we obtain $r = 2.6 \cdot 10^{-6}$ ms^{-1}. However, this value should be treated as a rough estimate–not only because the real kinetics are nonlinear, but most importantly because of the dependence of J on the crystal structure and orientation.

3.4. Splitting of the Fracture

[11] The computational bottleneck is the memory required to store the flow field and our calculations are currently limited to about $5 \cdot 10^6$ fluid nodes. The dissolving KDP fracture does not fit into this amount of memory at a resolution of 0.083 mm. To circumvent this difficulty we have divided the fracture into three overlapping pieces, each with length equal to the full fracture length and width equal to half the fracture width. The third piece, overlapping with the first two, is needed to eliminate the effects associated with the artificial boundary at $y = w/2$, y being the coordinate in the fracture plane perpendicular to the flow.

[12] Test calculations, together with the experimental and numerical results of *Hoefner and Fogler* [1988], have shown that at the beginning of the dissolution there is a very limited interaction between different areas of the fracture. The dissolution pattern at a given y_0 depends only on the topography in its immediate neighborhood $|y - y_0| < \delta$, with δ of the order of a few spatial correlation lengths. However, as the dissolution channels develop, the range of interaction increases. *Hoefner and Fogler* [1988] observed that channels interact when the difference in their lengths is of the order of the distance between them. When the difference in lengths is much larger than the distance between the channels, the flow in the shorter channel is substantially reduced and it ceases to grow.

[13] At $Pe = 216$, the interaction range, δ, remains less than $w/4$ to the end of the dissolution experiment. In this case the three sections can be combined to give the final dissolution pattern, but at $Pe = 54$ the interaction range grows quickly as soon as pronounced channels develop; in this case the pieces were combined at $\Delta h = 0.4h_0$. The dissolution simulation was continued with a coarser grid spacing of 0.166 mm, but since the fracture aperture has grown in the meantime, the reduced resolution still allows us to obtain the flow field with an acceptable accuracy. We have tested this process on smaller sections of the fracture and verified that the final dissolution pattern is not significantly affected by the rescaling to a coarser grid.
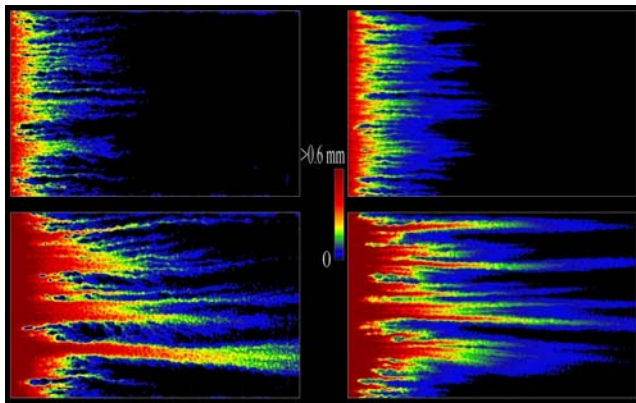
4. Results

[14] Figure 1 shows histograms of the aperture distribution at the beginning and end of the dissolution, obtained from experiment [*Detwiler et al.*, 2003] and numerical simulation. At $Pe = 54$ the distribution of small apertures is similar to the original distribution, indicating minimal dissolution in a substantial portion of the fracture, while the long tail corresponds to the rapid growth of pronounced dissolution channels during the experiment. In contrast, at $Pe = 216$ the entire distribution has shifted to larger apertures, indicating a more uniform dissolution, with the median aperture much larger than for the $Pe = 54$ experiment.

[15] These features of the experimental aperture distribution are well reproduced in the simulations with the exception of the tail of the simulated distribution at $Pe = 216$, which extends toward larger apertures than in the experimental case. Possible reasons for the discrepancy include the error associated with the finite amount of material taken away from the fracture surface in each step and the coarse resolution of the flow field.

[16] Figures 2 and 3 compare the dissolution patterns obtained by simulation and experiment at two different Peclet numbers. At $Pe = 216$ (Figure 2) the unsaturated fluid penetrates deep inside the fracture and the dissolution tends to be uniform throughout the sample, but at $Pe = 54$ (Figure 3) the erosion is slower and much more inhomogeneous, with a clearly visible dissolution front. This front becomes unstable with respect to fingering instabilities [*Ortoleva et al.*, 1987], since an increase in permeability within a channel enhances solute transport, leading to faster growth of the channel. As the dissolution proceeds, the channels compete for flow and the growth of the shorter channels eventually ceases. At the end of the experiment,
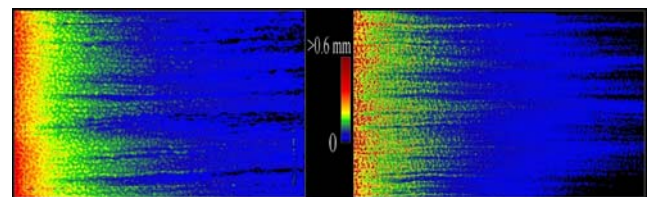
Figure 2. Aperture growth due to dissolution of a KDP fracture at $Pe = 216$. The figures show the dissolution patterns at $\Delta h = h_0$. The experimental result is shown on the left and the corresponding simulation result is on the right. The flow direction is from left to right.

Figure 3. Aperture growth due to dissolution of a KDP fracture at $Pe = 54$. The figures show dissolution patterns at (top) $\Delta h = 1/2 h_0$ and (bottom) $\Delta h = h_0$. The experimental results are shown on the left and the corresponding simulation results are on the right. The flow direction is from left to right.

the flow is focused in a few main channels while most of the pore space is bypassed.

[17] The experimental and numerical dissolution patterns are strikingly similar. At low Peclet number, the dominant channels (Figure 3) develop at the same locations in the simulation and experiment, despite the strongly nonlinear nature of the dissolution front instability. While there are differences in the length of the channels, relatively small changes (of the order of 10%) in the diffusion constant, D, or rate constant, r, can lead to comparable differences in the erosion patterns. Our results suggest that the simulations are capturing the effects of the complex topography of the pore space quite faithfully, despite the coarse aperture resolution in the flow solver.

5. Summary

[18] We have developed a fully microscopic numerical method to simulate the dissolution of rock fractures on experimentally relevant length scales. Dissolution morphologies similar to those seen experimentally have been observed. In particular, the strong dependence of the erosion patterns on Peclet number Pe is well reproduced. Algorithmic improvements now make it possible to simulate laboratory-scale flows, without the uncertainties introduced by lubrication approximations to the flow field or empirical mass-transfer coefficients. However, on larger scales approximate or up-scaled methods must still be used. Our results suggest that it will be possible to use microscopic simulations as an aid to the development and testing of Darcy scale models of dissolution.

References

Adler, P. M., and J.-F. Thovert (2000), *Fractures and Fracture Networks*, Springer, New York.

Békri, S., J.-F. Thovert, and P. M. Adler (1995), Dissolution in porous media, *Chem. Eng. Sci.*, *50*, 2765–2791.

Békri, S., J.-F. Thovert, and P. M. Adler (1997), Dissolution and deposition in fractures, *Eng. Geol.*, *48*, 283–308.

Brown, S. R., H. W. Stockman, and S. J. Reeves (1995), Applicability of the Reynolds equation for modeling fluid flow between rough surfaces, *Geophys. Res. Lett.*, *22*, 2537–2540.

Cheung, W., and H. Rajaram (2002), Dissolution finger growth in variable aperture fractures: Role of the tip-region flow field, *Geophys. Res. Lett.*, *29*(22), 2075, doi:10.1029/2002GL015196.

Detwiler, R. L., R. J. Glass, and W. L. Bourcier (2003), Experimental observations of fracture dissolution: The role of Peclet number in evolving aperture variability, *Geophys. Res. Lett.*, *30*(12), 1648, doi:10.1029/2003GL017396.

Dijk, P. E., B. Berkowitz, and Y. Yechieli (2002), Measurement and analysis of dissolution patterns in rock fractures, *Water Resour. Res.*, *38*(2), 1013, doi:10.1029/2001WR000246.

Dreybrodt, W. (1996), Principles of early development of karst conduits under natural and man-made conditions revealed by mathematical analysis of numerical models, *Water Resour. Res.*, *32*, 2923–2935.

Durham, W. B., W. L. Bourcier, and E. A. Burton (2001), Direct observation of reactive flow in a single fracture, *Water Resour. Res.*, *37*, 1–12.

Groves, C. G., and A. D. Howard (1994), Minimum hydrochemical conditions allowing limestone cave development, *Water Resour. Res.*, *30*, 607–615.

Hoefner, M., and H. Fogler (1988), Pore evolution and channel formation during flow and reaction in porous media, *AIChE J.*, *34*, 45–54.

Koziejowska, A., and K. Sangwal (1988), Surface micromorphology and dissolution kinetics of potassium dihydrogen phosphate (KDP) crystals in undersaturated aqueous solutions, *J. Mater. Sci.*, *23*, 2989–2994.

Nicholl, M. J., H. Rajaram, R. J. Glass, and R. L. Detwiler (1999), Saturated flow in a single fracture: Evaluation of the Reynolds equation in measured aperture fields, *Water Resour. Res.*, *35*, 3361–3373.

Ohara, M., and R. C. Reid (1973), *Modelling Crystal Growth Rates from Solutions*, Prentice-Hall, Upper Saddle River, N. J.

Oron, A. P., and B. Berkowitz (1998), Flow in rock fractures: The local cubic law assumption reexamined, *Water Resour. Res.*, *34*, 2811–2825.

Ortoleva, P., J. Chadam, E. Merino, and A. Sen (1987), Geochemical self-organisation II: The reactive-infiltration instability, *Am. J. Sci.*, *287*, 1008–1040.

Szymczak, P., and A. J. C. Ladd (2004), Stochastic boundary conditions to the convection-diffusion equation including chemical reactions at solid surfaces, *Phys. Rev. E.*, *69*, 036704.

Verberg, R., and A. J. C. Ladd (1999), Simulation of low-Reynolds-number flow via a time-independent lattice-Boltzmann method, *Phys. Rev. E*, *60*, 3366–3373.

Verberg, R., and A. J. C. Ladd (2000), Lattice-Boltzmann model with sub-grid scale boundary conditions, *Phys. Rev. Lett.*, *84*, 2148–2151.

Verberg, R., and A. J. C. Ladd (2002), Simulations of erosion in narrow fractures, *Phys. Rev. E*, *65*, 056311.

————————
A. J. C. Ladd, Chemical Engineering Department, University of Florida, Gainesville, FL 32611-6005, USA. (ladd@che.ufl.edu)

P. Szymczak, Institute of Theoretical Physics, Warsaw University, Hoża 69, 00-618, Warsaw, Poland.